



Stockholm
University

Bachelor Thesis

Degree Project in
Geology 15 hp

Fault-slip analysis southeast of the Troodos massif. Implications for the uplift of the Troodos mountains

Hermes Pantazidis



Stockholm 2017

Department of Geological Sciences
Stockholm University
SE-106 91 Stockholm

CONTENTS

ABSTRACT	2
1. INTRODUCTION	3
2. TECTONIC SETTING OF CYPRUS	6
2.1 FAULT ZONES	8
3. METHODS	10
3.1 MEASUREMENTS	10
3.2 PROCESSING OF DATA	10
3.3 MAPS	10
4. RESULTS	11
1) ARAKAPAS FAULT ZONE	12
2) YERASA FAULT ZONE	13
3) KALAVASOS FAULT ZONE	17
4) TOCHNI FAULT ZONE	18
5) WENOGEIA FAULT ZONE	19
6) SKARINOI FAULT ZONE	19
4.1 SUMMARY AND INTERPRETATION OF FAULT-SLIP DATA	22
5. DISCUSSION	23
5.1 COMPARISON WITH THE OVGOOS FAULT ZONE	23
5.2 CONFLICTING DATA	25
5.3 IMPLICATIONS FOR FUTURE STUDIES	26
6. CONCLUSION	27
ACKNOWLEDGEMENTS	27
REFERENCES	28
APPENDIX	28

Abstract

North-south compression has been influencing Cyprus at least since the early Pliocene. This compression is responsible for uplift in the area and contractional tectonism along E-W striking fault zones. In the Pleistocene (1.5-2 Ma), the collision between the Eratosthenes seamount and Cyprus possibly caused an increased uplift on the Troodos mountains. The study provides evidence from fault-slip data that the fault zones in the southeast of Troodos were caused due to the collision between the Eratosthenes seamount and Cyprus. It is further discussed that the stratigraphic age of the bedrocks hosting the fault zones could be as young as Messinian (5-6 Ma). The Fault-slip data showed no more than one movement event in most fault zones which may be broadly linked to the collision event. Finally, the study discusses the difference in uplift between the Troodos mountains and the Kyrenia range in the North of Cyprus to conclude that, the event of the collision between the Eratosthenes seamount and Cyprus could be linked to the increased uplift of the Troodos mountains.

1. Introduction

The complex tectonic setting of Cyprus between the African and Eurasian plate influenced its geological evolution for the past 180 million years (Ma). More recently, (since 10-20 Ma) Cyprus is under the influence of the Cypriot arc. The Cyprus arc is an east-west striking, convergence point between the African and Eurasian plates. The African plate subducting under the Eurasian plate caused N-S compression at least since the early Pliocene. This caused an uplift of the area and contractional tectonism along E-W-striking fault zones (Harrison *et al.*, 2004). In the Pleistocene, the Eratosthenes seamount south of the Cyprus arc functioned as a promontory of the African plate and collided with Cyprus. The Eratosthenes seamount is a carbonate platform that formed in the Cretaceous (Yossi mart, Robertson, et al 1998). The collision of this, relatively small seamount caused increased uplift in a limited area in front of the seamount (Robertson, 1998). There is a distinct spatial connection between the position of seamount collision and the uplift causing the Troodos mountains (Figure 1). The uplift of the ophiolitic sequences of the Troodos terrane cause differential vertical movement that has been accommodated by a series of fault zones. These fault zones are indicators of the drastic change in relief on the landscape. The Troodos massif is towering over the surrounding area that consists of young sediments (middle to upper Miocene), (Kinnaird, Robertson and Morris, 2011) that are elevation wise very close to that of sea level (Figure 1).

This study presents some important aspects for the following reasons: (1) The complex tectonic history of Cyprus makes the different fault zones in the area hard to link to specific events. (2) The landscape of the Troodos massif and surrounding area underwent a drastic change since the collision of the Eratosthenes seamount, which is structurally not understood. Fault-slip analysis of the southeast corner of the Troodos uplift could possibly reveal more information on the kinematics of the Troodos mountains. The Troodos uplift is an event that has been studied by different disciplines of geology. In the structural geology discipline there have been studies in the west side of Troodos (Varga, 1991) but no detailed studies of the kinematics in the complex fault zone network.

The educational aspects are: (1) The recognition and measurement of the movement indicators on fault zones and (2) Implementation of structural tools for the representation and expression of the measurements taken in a scientific way. In a practical aspect, measurements from the southeast side of the Troodos massif were taken only on fault planes on which the sense of relative movement could be

recognized. The rationale is that this allows the computation of the principal strain axes ($X > Y > Z$) or ($1 > 2 > 3$) on a regional scale for relation of this information to N-S shortening exerted by the collision of the Eratosthenes seamount. The main goals of the analysis are: (1) the constraint of the kinematics of variably oriented fault zones in the southeast corner of the Troodos uplift. (2) the constraint of the timing of the fault zone kinematics using the stratigraphic ages of bedrocks that have been faulted and (3) to unearth possible correlations between the N-S compression and the Eratosthenes seamount collision with the uplift of Troodos massif.

Cyprus and its relative position to the Eratosthenes seamount

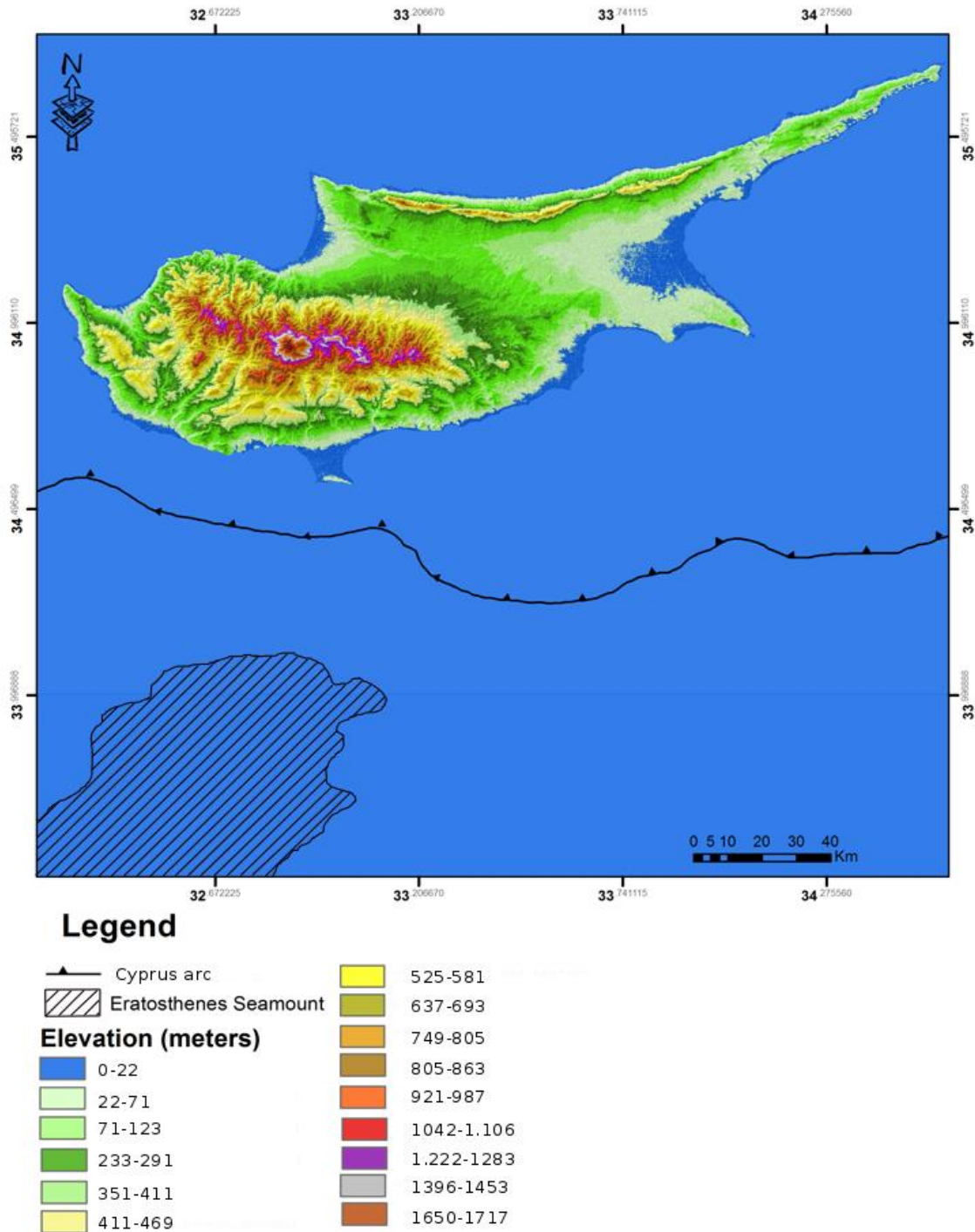


Figure 1: Digital elevation map of Cyprus and the relative position to the Eratosthenes seamount and the subduction zone south of it. NASA JPL. (2013). NASA Shuttle Radar Topography Mission Global 1 arc second [Data set]. NASA LP DAAC. <https://doi.org/10.5067/MEaSUREs/SRTM/SRTMGL1.003>

2. Tectonic setting of Cyprus

Cyprus is situated close to the meeting point of three tectonic plates: The African, Eurasian and Arabian plates. A wide variety of tectonic processes are situated in the region like: obduction, subduction and transform faulting. These processes take place in the margins of the previously mentioned tectonic plates. Since the Mesozoic, these processes formed several fragmented tectonic terranes such as: Cyprus, the Hellenic arc, the Aegean graben system and the Anatolian microplate (Mart and Ryan, 2002) The tectonic framework is complicated and the main theory behind the larger motion of forces in the Cyprus arc as explained by Yosi Mart and William B.F. Ryan (1998). The review refers to the most common regime which is that the African plate moving to the north and the Eurasian plate, moving to the south create a compressional zone. It is believed that the N-S compression started at least in the early Pliocene (Harrison *et al.*, 2004) and caused E-W striking fault zone trends such as the Ovgos fault in northern Cyprus (R.W Harrison et al 2002) (Figure 2). The Cyprus arc is a product of this compressional zone and so is the uplift in the area. The arc is a subduction zone where the African plate subducts under the Eurasian plate (R.W Harrison et al 2002). South of the subduction zone lies the Eratosthenes seamount. The Eratosthenes seamount is a carbonate platform and plays an important role in the uplift of the Troodos ophiolite, as geophysical data and plate kinematics support the claim that the Eratosthenes seamount collided with Cyprus and caused an increased uplift of the Troodos massif. The collision which occurred around 1.5 to 2 Ma ago not only caused an uplift effect on Cyprus but also a subsidence on the Eratosthenes seamount (Kempfer, 1998). The geology and origins of the Eratosthenes seamount are unclear, since deeper drilling is needed in order to go further back in time. The drilling in the seamount that was taken during Leg 160 dated lithological data back to the early cretaceous. Further geological and geophysical data support the evidence that the seamounts tectonic evolution was the same as the North African continental margin from early Mesozoic and forward (Robertson et al 1998). In late cretaceous a subsidence of the seamount occurred to bathyal depths. Prior to that, it was an early cretaceous shallow-marine deposit (Robertson et al 1998). Miocene limestone data from Sites 965 and 966(leg 160) showed that the seamount was subjected to an uplift at that time. More recently in Pliocene-Pleistocene time the seamount was thrust below Cyprus due to the African-Eurasian plate collision (Robertson et al 1998). The subsidence of the seamount fit the spatial connection with the uplift of Troodos massif. In figure 1 it can be seen that the Troodos massif has a large elevation difference with

the Upper Miocene sediments surrounding it in the southeast, south, and east. That is something that could be a result of the differential vertical movement of the massif in comparison to the surrounding Upper Miocene sediments. The study area is located south and southeast of the massif. Since the massif has been uplifted higher than the surroundings we would expect normal fault zones throughout their border with the massif, where the vertical movement took place. The study area was divided into six areas, where each area represents a different fault zone. All the fault zones are represented on the DEM maps in the results section (figure 3). The fault zones also appear in a geological map of Cyprus (see geological map in appendix).

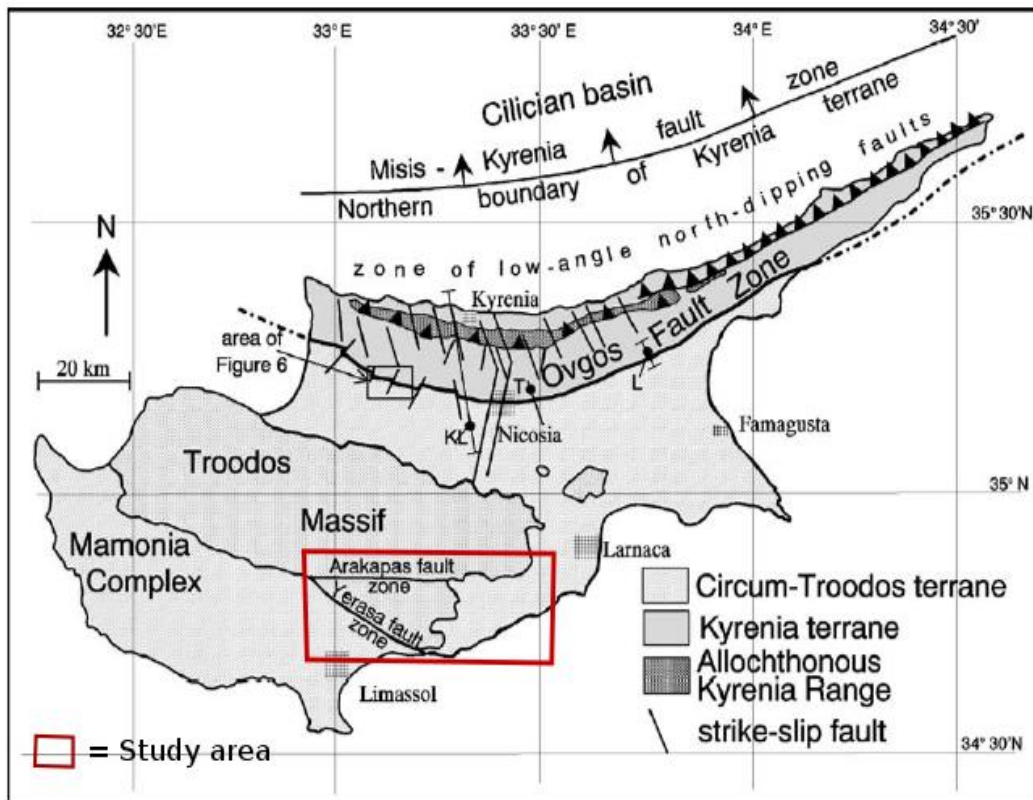


Figure 2: Generalized tectonic map of Cyprus. Important aspects are: a) The E-W striking fault zone in Arakapas. b) The E-W striking fault zone of Ovgos. Both of these fault zones possibly caused by N-S compression. Map modified from (R.W Harrison et al 2002).

2.1 Fault zones

The study area consists of the following 6 fault zones (Figure 3): (1) The Arakapas fault zone which is an East-West striking fault zone. The bedrock that hosts the fault zone has different rock types such as: Diabasic, dykes, serpentinite, dating to Upper Cretaceous (Campanian). (2) The Yerasa fault zone which is a Northwest-Southeast striking fault zone with bedrock that consists of: Serpentinite (Upper Cretaceous) and sediments dating from Palaeogene to Upper Miocene like: marls, chalks, and different biostrome reef limestones. (3) The Kalavastos fault zone which is a North-south striking fault zone hosted by a sedimentary bedrock dating from Palaeogene to Upper Miocene, with marls, chalks and different biostrome reef limestones. (4) The Tochni fault zone which is also a North-south striking fault zone with sedimentary bedrock dating from Palaeogene to Upper Miocene with chalks, marls, reef limestones and also gypsum dating specifically to Upper Miocene. The gypsum deposits on the Tochni fault zone are a product of the Messinian salinity crisis. (5) The W-E striking Wenogeia fault zone. The bedrock hosting this fault consists of Upper Cretaceous originated pillow lavas and of chalks and marls dating from the Palaeogene. (6) The Skarinou fault zone which strikes North-south and has a bedrock consisting of Palaeogene to upper Miocene sedimentary rocks: chalks, marls and biostrome reef limestones.

Study area fault zones

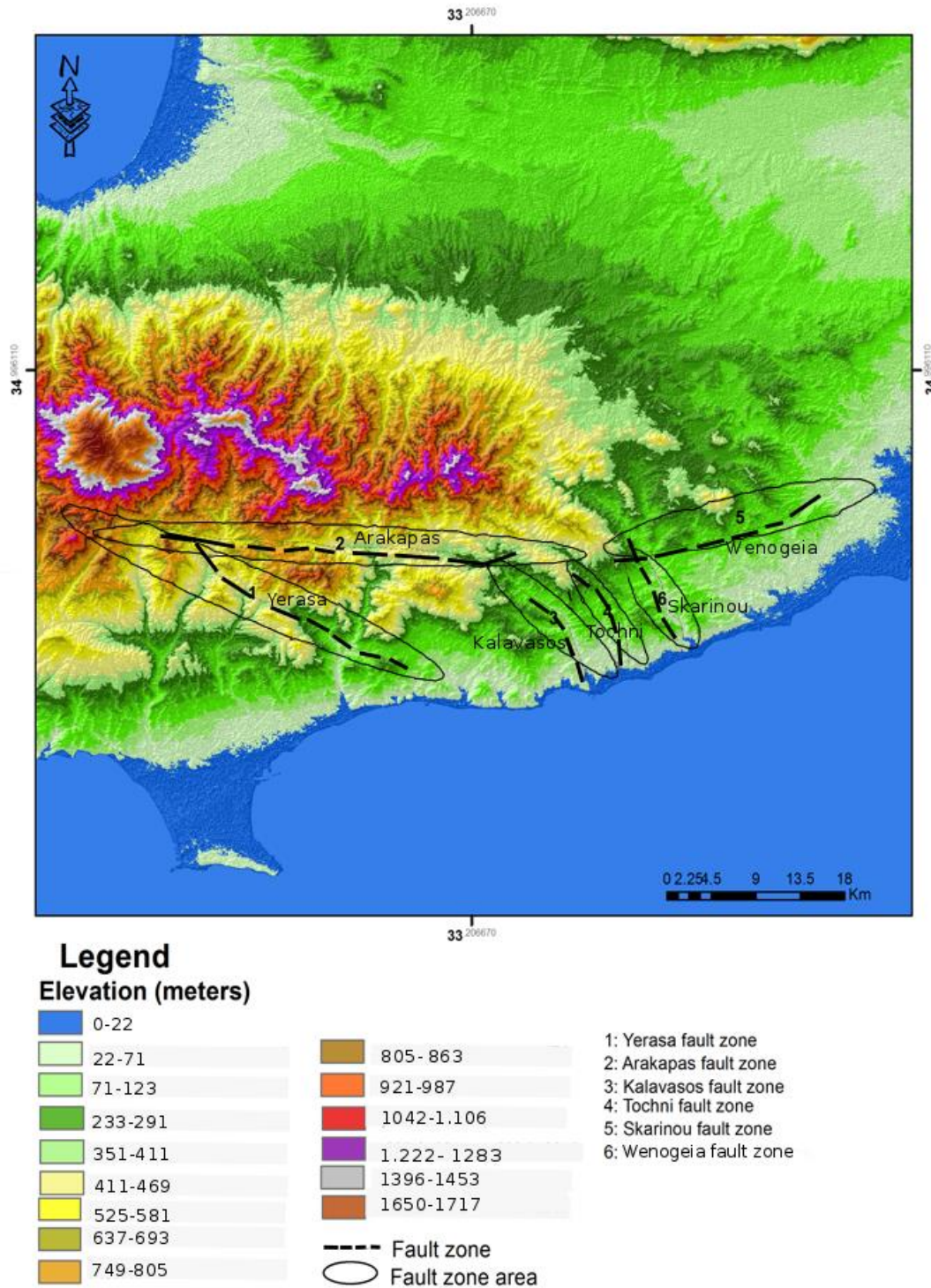


Figure 3: Digital elevation map of the study area, fault zone locations and areas are presented. NASA JPL. (2013). NASA Shuttle Radar Topography Mission Global 1 arc second [Data set]. NASA LP DAAC. <https://doi.org/10.5067/MEaSURES/SRTM/SRTMGL1.003>

3. Methods

3.1 Measurements

While in the field (Figure 3) the focus was on identifying fault planes with striations on them. After that, detection and measurement of movement indicators such as stepped fibres on the fault planes and Riedel shears within the fault plane (Petit, 1987) was the next task. Measurements on fault planes that showed no movement indicators were not taken. Dip and dip direction measurements were taken first, followed by lineation measurements. A total of 54 outcrops were visited. An average of 15 dip and dip direction and 15 lineation measurements per outcrop were obtained. Two geological compasses were used as tools. GPS Coordinates (WGS 84) were acquired in the location of the outcrops. In general terms, fibre and striae orientations on slickensides from the studied fault zones were simple and consistent, readily interpretable with the geometry of the mapped faults at a regional scale. There was no evidence for multiple movement events in the studied fault zones.

3.2 Processing of data

The data processing was done using the Faultkin program and its various tools (R.W. Allmendinger 2006-2016). The data was transferred manually to the Apache Open office spreadsheet program (Apache software foundation) and then imported to Faultkin. The data were plotted in lower hemisphere projections. Finally linked Bingham distribution eigenvalues were also calculated for each outcrop. Through this processing the distribution of the number of movement indicators over a number (three planes in this occasion) of axes is achieved. Facilitating the identification of a pattern in the extension or shortening direction. The projections were later processed in the program Inkscape. North direction, the number of measurements along with extension or shortening indicators (in the form of arrows) were given to each stereonet projection.

3.3 Maps

Digital elevation maps were created with the ARCGIS program based on raw SRTM data received by US geological survey website. Four DEM (digital elevation map) maps were created: (1) Dem map of Cyprus, (2) Dem map of the study area showcasing the fault zones, and (3,4) Dem maps of the study area marked with each outcrop location for a better understanding of movement. Every outcrop had its coordinates written down and then imported on ARCGIS in an excel file to pinpoint the exact location.

4. Results

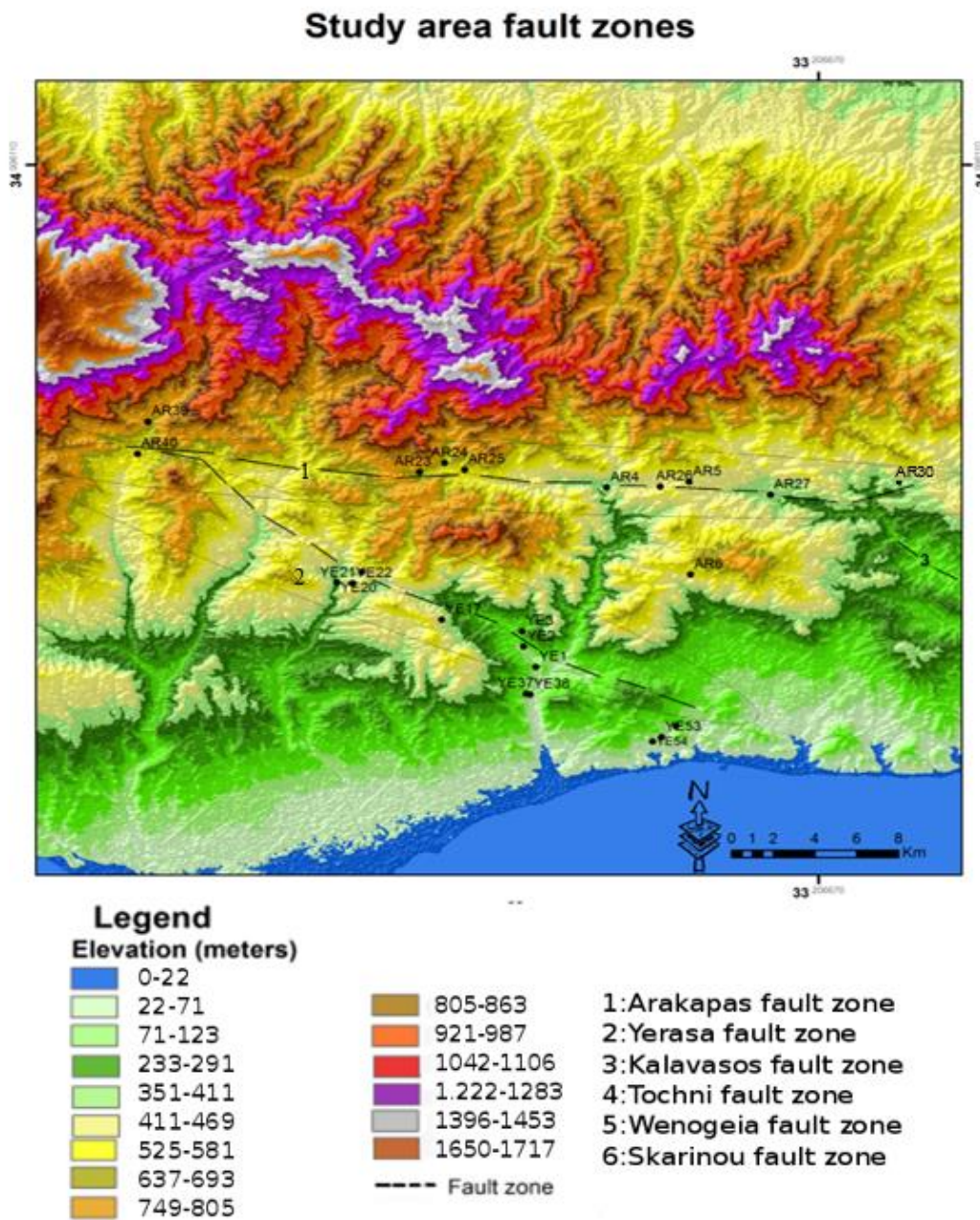


Figure 4: Digital elevation map over the study area showcasing the location of outcrops visited. Each outcrop has a code of the area and number of visit. NASA JPL. (2013). NASA Shuttle Radar Topography Mission Global 1 arc second [Data set]. NASA LP DAAC. <https://doi.org/10.5067/MEaSURES/SRTM/SRTMGL1.003>

1) Arakapas fault zone

N-S shortening together with W-E extension are evident from the Arakapas fault zone results. The N-S shortening, W-E extension and N-S extension are being supported by three (AR4, AR5, AR26), five (AR6, AR24, AR40, AR30, AR27) and four (AR25, AR39, AR23) outcrops, respectively.

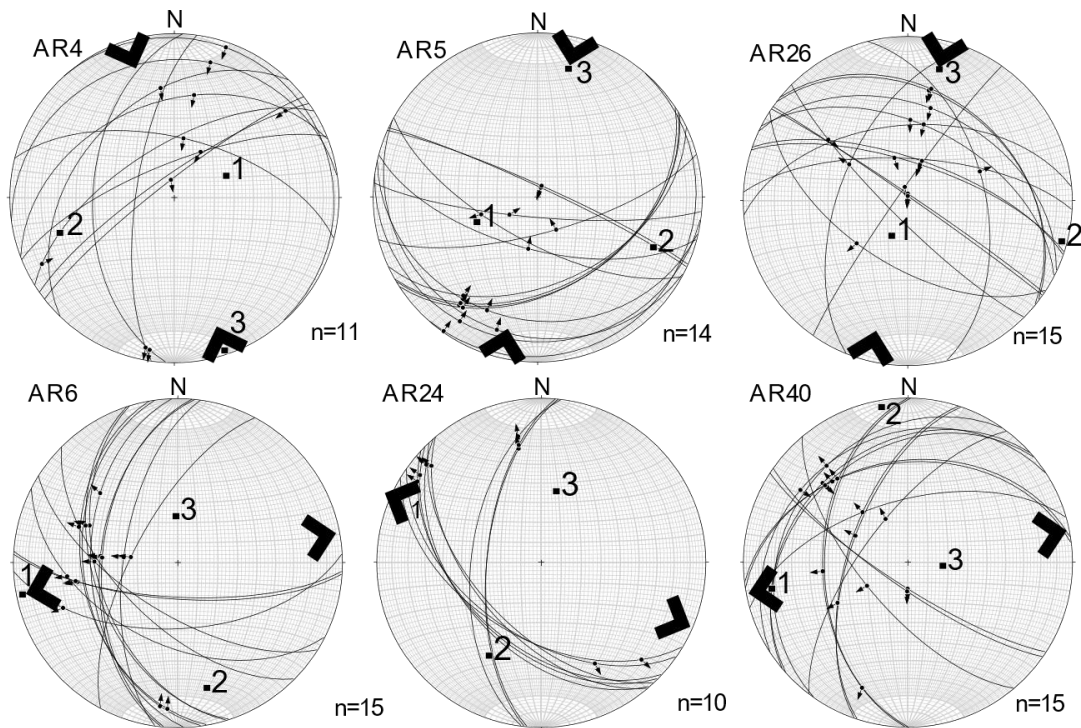


Figure 5: Fault slip data from the Arakapas fault zone. Stereonets are lower hemisphere equal area projections. Fault planes represented by great circles and projected trace of lineation by small arrows. Principal strain axes ($1 > 2 > 3$) $1=X$, $2=Y$, $3=Z$. Extension and Shortening expressed by arrows on the outside of stereonets. **AR4:** nine thrusts dipping to the north. North-south shortening overall. Two sinistral strike slip faults. **AR5:** Eleven thrusts dipping to the south, one thrust dipping to the north. North-south shortening overall. One normal fault. **AR26:** 11 thrusts dipping to the north. Overall north-south shortening. Two normal faults dipping to northwest and southwest. One normal fault dipping to the east. One sinistral strike slip. **AR6:** ten normal faults dipping to the west. Three normal faults dipping to the south. Two thrusts dipping the west. Overall west-east extension. **AR24:** 7 normal faults dipping to the southwest. Three normal faults dipping to the west. Overall northwest-southeast extension. **AR40:** Six normal faults dipping to the northwest. Two normal faults dipping to the west. Overall west east extension. Two normal faults dipping to the southwest. Two thrusts dipping to the northwest.

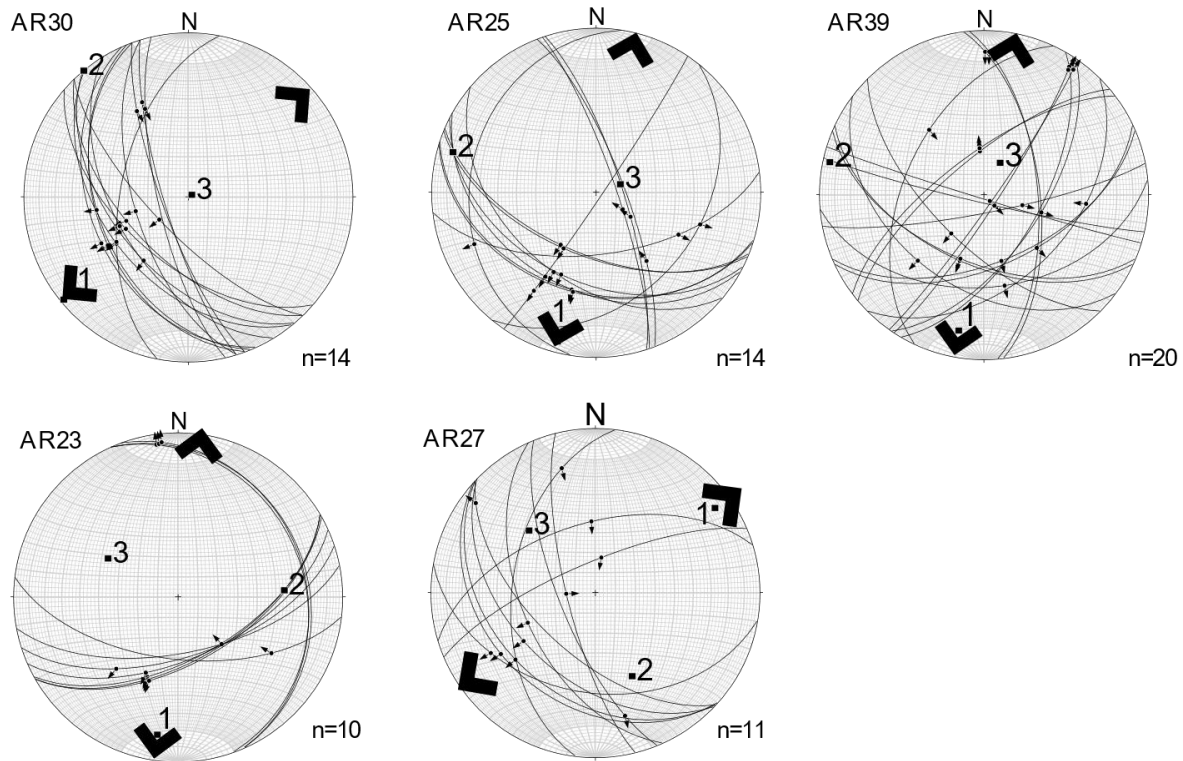


Figure 5: (continued) **AR30:** Ten normal faults dipping to the southwest. Overall southwest-northeast extension. Three sinistral strike slip faults dipping to the west. **AR25:** Seven normal faults dipping to the southwest. One normal fault dipping to the west. One normal fault dipping to the south. Overall northeast- southwest extension. Three thrusts dipping to the northeast. One sinistral strike slip fault. **AR39:** four normal faults dipping to the southwest. Five normal faults dipping to the southeast. Two normal faults dipping to the northwest. Overall Northeast-southeast extension. Three dextral strike slip faults dipping to the southeast. One thrust dipping to the southeast. One thrust dipping to the northwest. **AR23:** Five normal faults dipping to the southeast. Three normal faults dipping to the west. Overall north-south extension. Two thrusts dipping to the northwest and northeast. **AR27:** Five normal faults dipping to the southwest. Two thrusts dipping to the northwest and one thrust dipping to the west. Overall northeast-southwest extension. Two sinistral strike slip faults dipping to the southwest.

2) Yerasa fault zone

W-E extension accompanied by N-S Shortening was mainly showed from the Yerasa fault-slip analysis. The W-E extension and N-S shortening are being supported from (YE22, YE3, YE20, YE18, YE54, YE52, YE17, YE19) and three (YE1, YE2, YE21) outcrops, respectively. N-S extension of a small extent was apparent from the fault-slip data results.

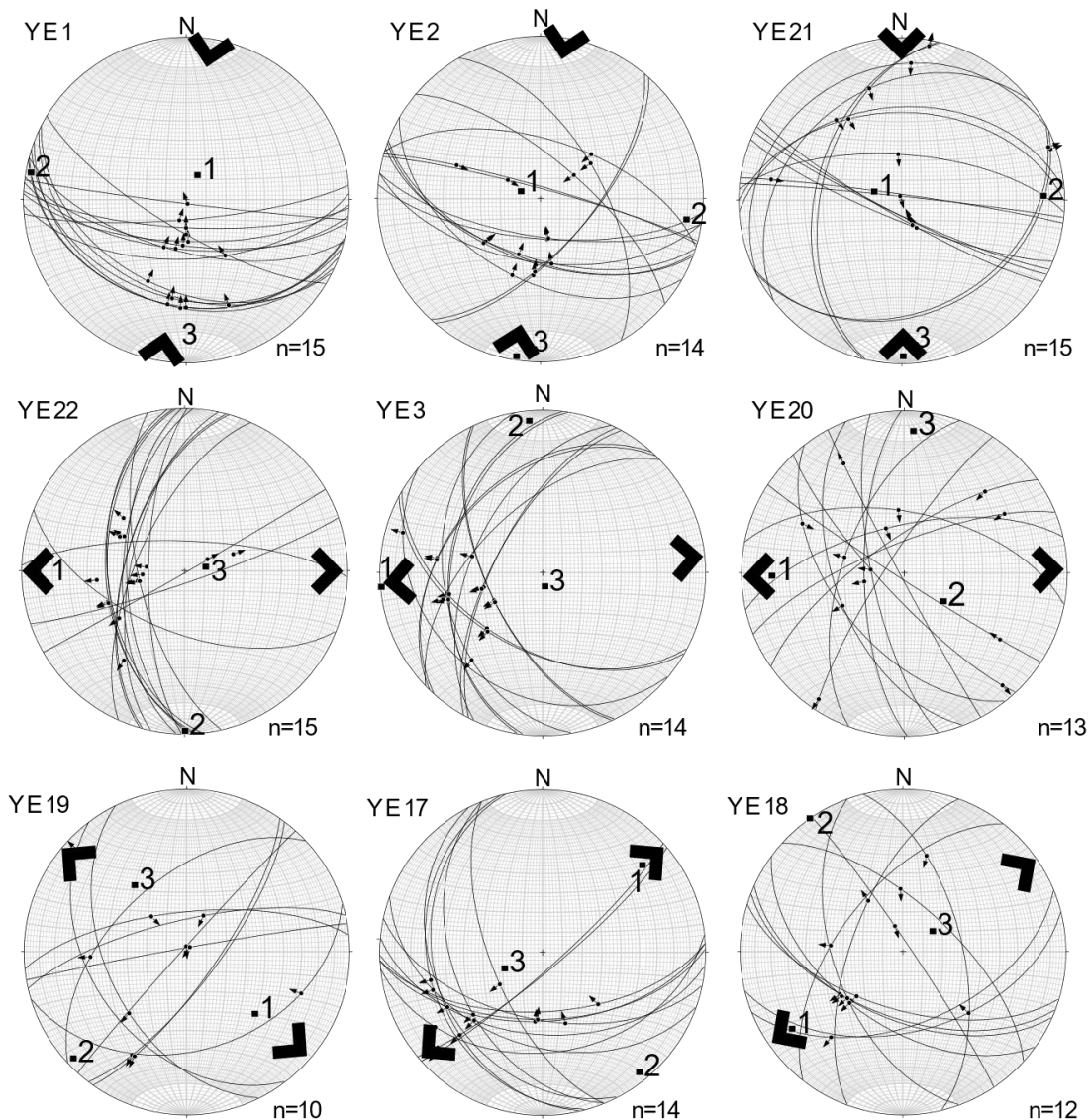


Figure 6: Fault slip data for Yerasa fault. **YE1:** fifteen thrusts dipping to the south. Overall north-south shortening. **YE2:** seven thrusts dipping to the south. Two thrusts dipping to the west. Three thrusts dipping to the northeast. North-south shortening overall. Two dextral strike slip faults. **YE21:** Seven thrusts dipping to the north. One thrust dipping to the west. Four thrusts dipping to the south. Overall north-south shortening. One normal fault dipping to the west. Two normal faults dipping to the east. The last two normal faults indicate a west-east extension. One dextral strike slip fault dipping to the north. **YE22:** twelve normal faults dipping to the west. One normal fault dipping to the southwest. Overall west-east extension. Two dextral strike slip faults. **YE3:** Five normal faults dipping to the southwest. Nine normal faults dipping to the northwest. West-east extension overall. **YE20:** Four normal faults dipping to the west/northwest. Four thrusts dipping to the northwest/north. Overall west east extension. One thrust dipping to the west. Two sinistral strike slip faults. One dextral strike slip fault. One dextral strike slip fault dipping to the northwest. **YE17:** Six normal faults dipping to the south-west. Five thrusts dipping to the south. Three sinistral strikes slip faults dipping to the south-east. Overall north-east to south-west extension. Dipping to the south-east. Three thrusts dipping to the north. Overall extension to north-west to south-east. One thrust dipping to the north-west. **YE18:** Five normal faults dipping to the south-west. Two normal faults dipping to the north-west. Overall extension south-west to north-east. Three thrusts dipping to the north-east. One thrust dipping to the south-east. One normal fault dipping to the south-east. **YE19:** Three normal faults dipping to the south-west. Two thrusts dipping to the north, one thrust dipping to the south-east. Overall northwest-southeast extension.

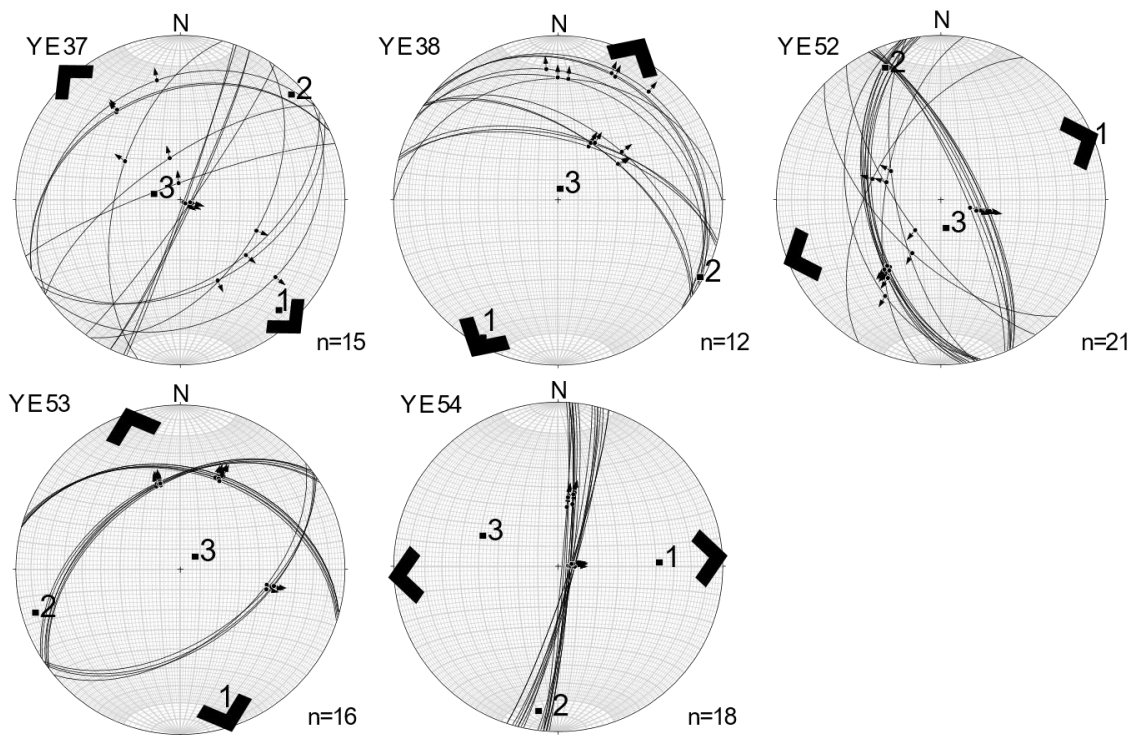


Figure 6: (continued) **YE37:** Six normal faults dipping to the north-west. Nine normal faults dipping to the south-east. Overall north-west to south-east extension. **YE38:** Twelve normal faults dipping to the north-east. Overall north-east to south-west extension. **YE52:** Three normal faults dipping to the north-west. Fourteen normal faults dipping to the west. Seven normal faults dipping to the north-east. Overall extension north-east to south-west. **YE53:** Six normal faults dipping to the north-west. Five normal faults dipping to the north-east. Four normal faults dipping to the south-east. Overall extension north-west to south-east. **YE54:** Seven normal faults dipping to the east. Overall west-east extension. Eight dextral strike slip faults dipping to the east.

Study area fault zones

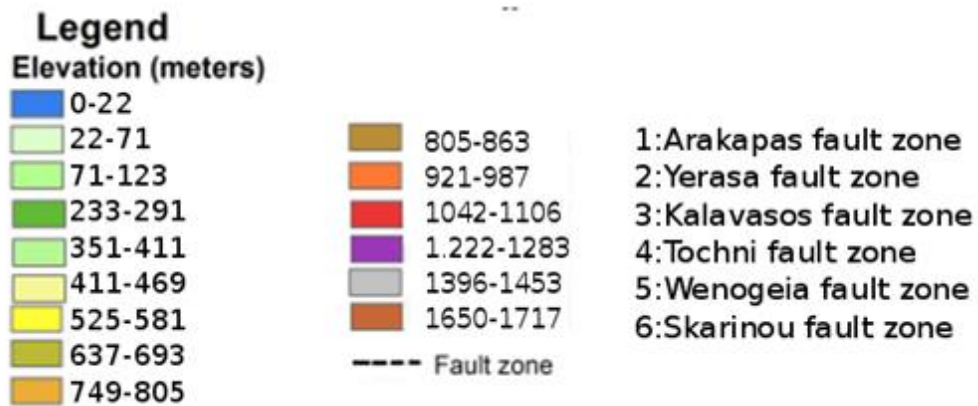
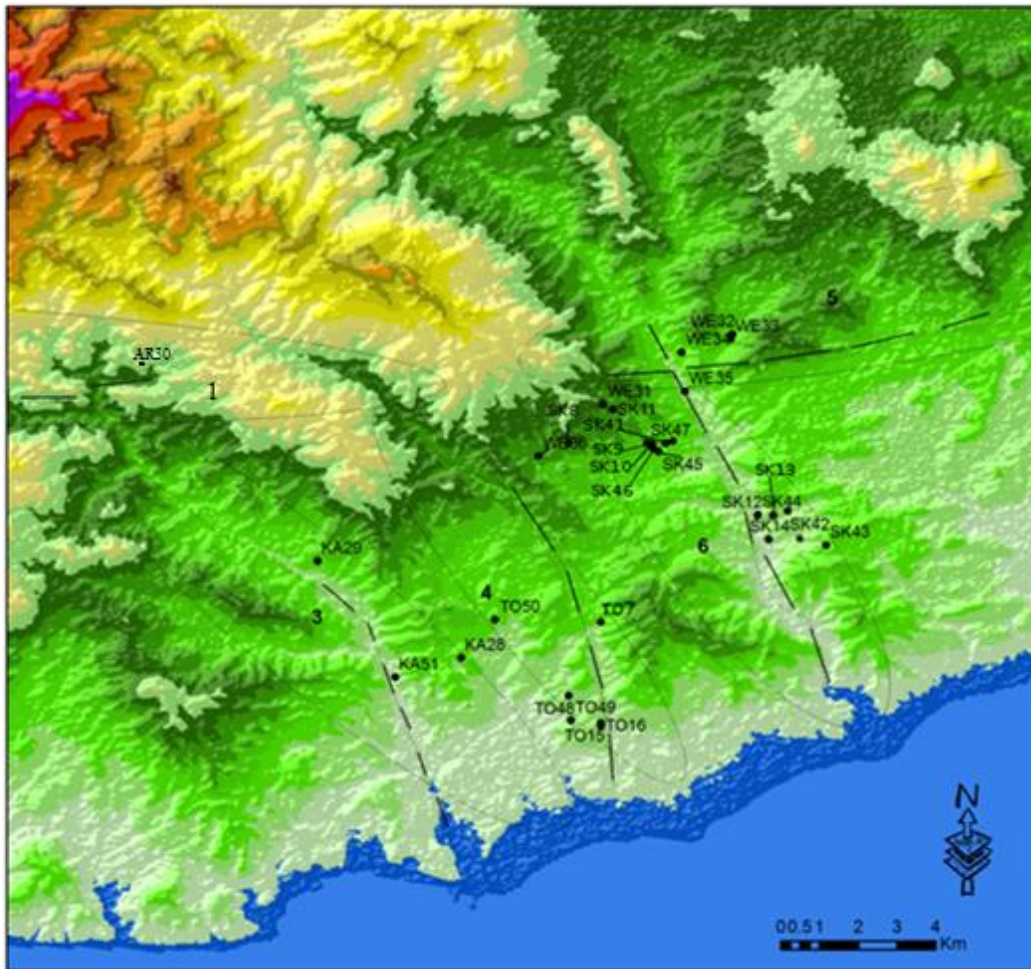


Figure 7: Digital elevation map of the study area. Every outcrop has an area code and visit number. NASA JPL. (2013). NASA Shuttle Radar Topography Mission Global 1 arc second [Data set]. NASA LP DAAC. <https://doi.org/10.5067/MEaSURES/SRTM/SRTMGL1.003>

3) Kalavassos fault zone

Two main patterns emerge from the Kalavassos fault-slip data results, W-E extension and W-E shortening based on outcrop Ka29 and outcrops Ka51 and Ka28, respectively.

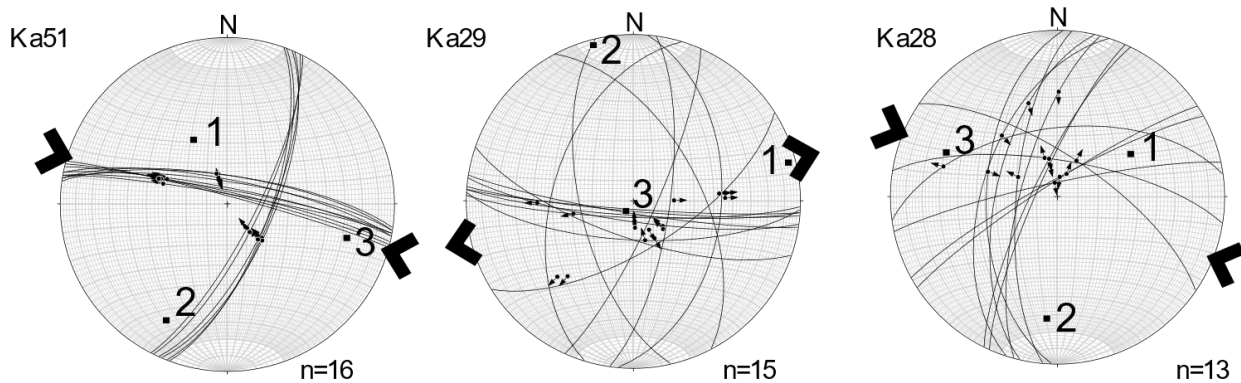


Figure 8: Fault slip data for Kalavassos fault zone. **KA51:** Six thrusts dipping to the south-east. Three thrusts dipping to the north-east. Overall south-east to north-west shortening. One normal fault dipping to the north-east. Six sinistral strike slip faults dipping to the north-east. **KA29:** Three normal faults dipping to the east. Two normal faults dipping to the west. Three normal fault dipping to the south. One thrust dipping to the south-west. Three thrusts dipping to the south. One sinistral strike slip fault dipping to the south. Overall north-east to south-west extension. **KA28:** Four thrusts dipping to the north-west. Four thrusts dipping to the west. Two normal fault dipping to the north-west. One normal fault dipping to the north-east. One normal fault dipping to the west. One normal fault dipping to the north. Overall south-east to north-west shortening.

4) Tochni fault zone

W-E extension was shown from the Tochni fault-slip data results derived from 4 outcrops (TO7, TO50, TO16, TO15). N-S extension is being supported from fault-slip data results from two outcrops (TO49, TO48).

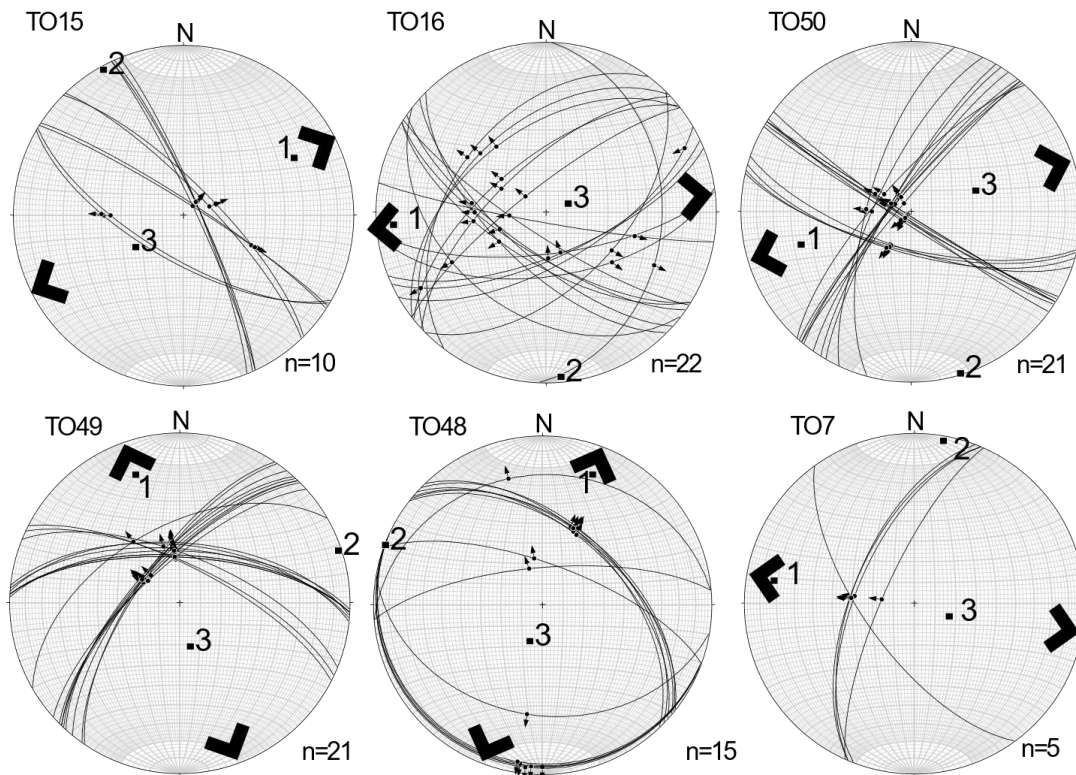


Figure 9: Fault slip data for Tochni fault zone. **TO15:** Two normal faults dipping to the south-west. Eight normal faults dipping to the north-east. Overall north-east to south-west extension. **TO16:** Four normal faults dipping to the south-east. Seven normal faults dipping to the north-west. Four normal faults dipping to the south-west. Three thrusts dipping to the south-east. Overall west-east extension. **TO50:** Ten normal faults dipping to the north-west. Eleven normal faults dipping to the south-west. Overall north-west to south-west extension. **TO49:** Ten normal faults dipping to the north-west. Six normal faults dipping to the north. Three normal faults dipping to the north-east. Overall north-west to south-east extension. **TO48:** Seven normal faults dipping to the north-east. Two normal faults dipping to the north. Six normal faults dipping to the south. Overall north-east to south-west extension. **TO7:** One normal fault dipping to the south-west. Four normal faults dipping to the north-west. Overall north-west to south-east extension.

5) Wenogeia fault zone

Two main patterns are being showcased from the Wenogeia fault zone data results. First dominant N-S shortening and secondly W-E extension are being supported on four outcrops (WE31, WE32, WE35, WE36) and two outcrops (WE33, WE34), respectively.

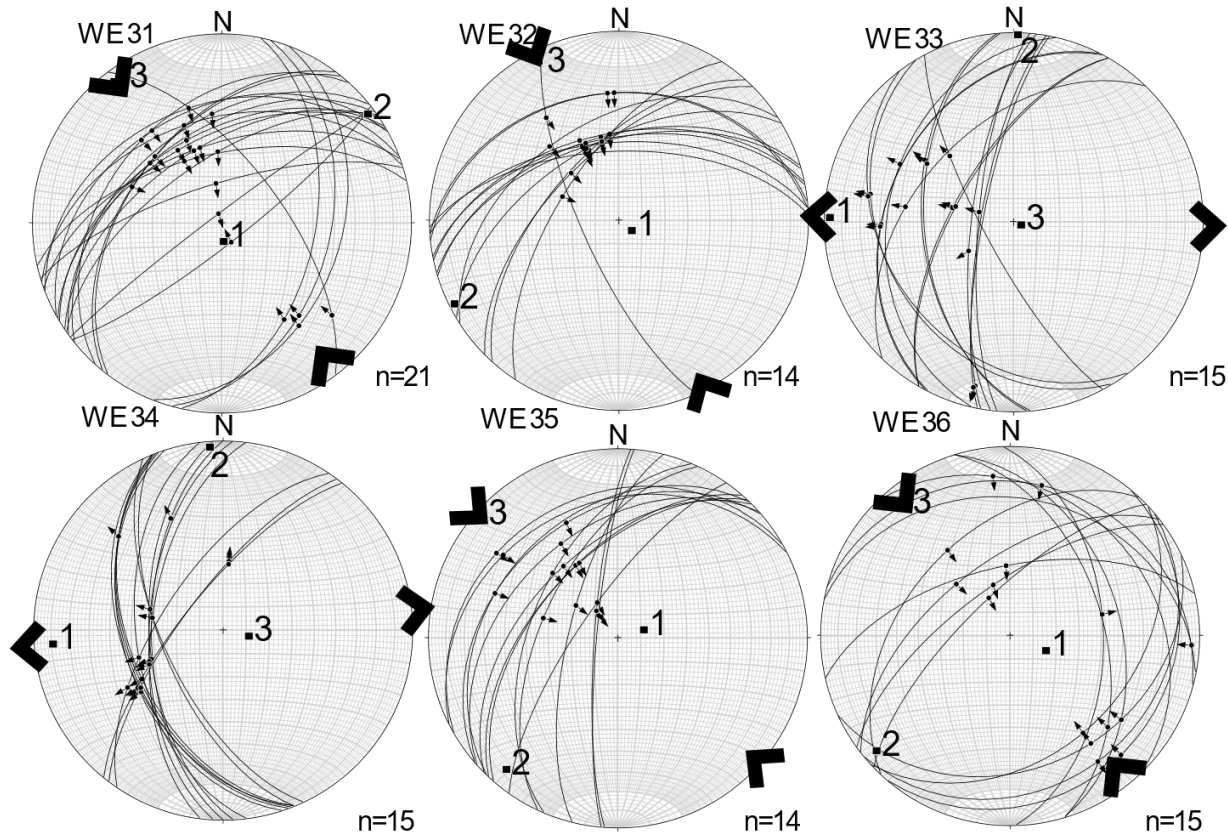


Figure 10: Fault slip data for Wenogeia fault zone **WE31:** Sixteen thrusts dipping to the northwest. Four thrusts dipping to the east. One thrust dipping to the northwest. Overall northwest-southeast shortening. **WE32:** One thrust dipping to the southwest. Thirteen thrusts dipping to the northwest. Overall northwest-southeast shortening. **WE33:** fifteen faults dipping to the west. Overall west-east extension. **WE34:** Three faults dipping to the northwest. Twelve faults dipping to the west. Overall west-east extension. **WE35:** Fourteen thrusts dipping to the northwest. Overall northwest-southeast shortening. **WE36:** Five thrusts dipping to the northwest. Three thrusts dipping to the northeast. Five thrusts dipping to the southeast. Overall northwest-southeast shortening. One normal fault dipping to the southeast. One normal fault dipping to the west.

6) Skarinou fault zone

Two patterns became apparent by fault-slip data results from Skarinou fault zone. W-E extension is being showcased by eight outcrops (SK44, SK45, SK42, SK13, SK12, SK10, SK8, SK9), N-S extension is being showcased by four outcrops (SK47, SK43, SK41, SK14) and W-E Shortening is being showcased by one outcrop (SK46).

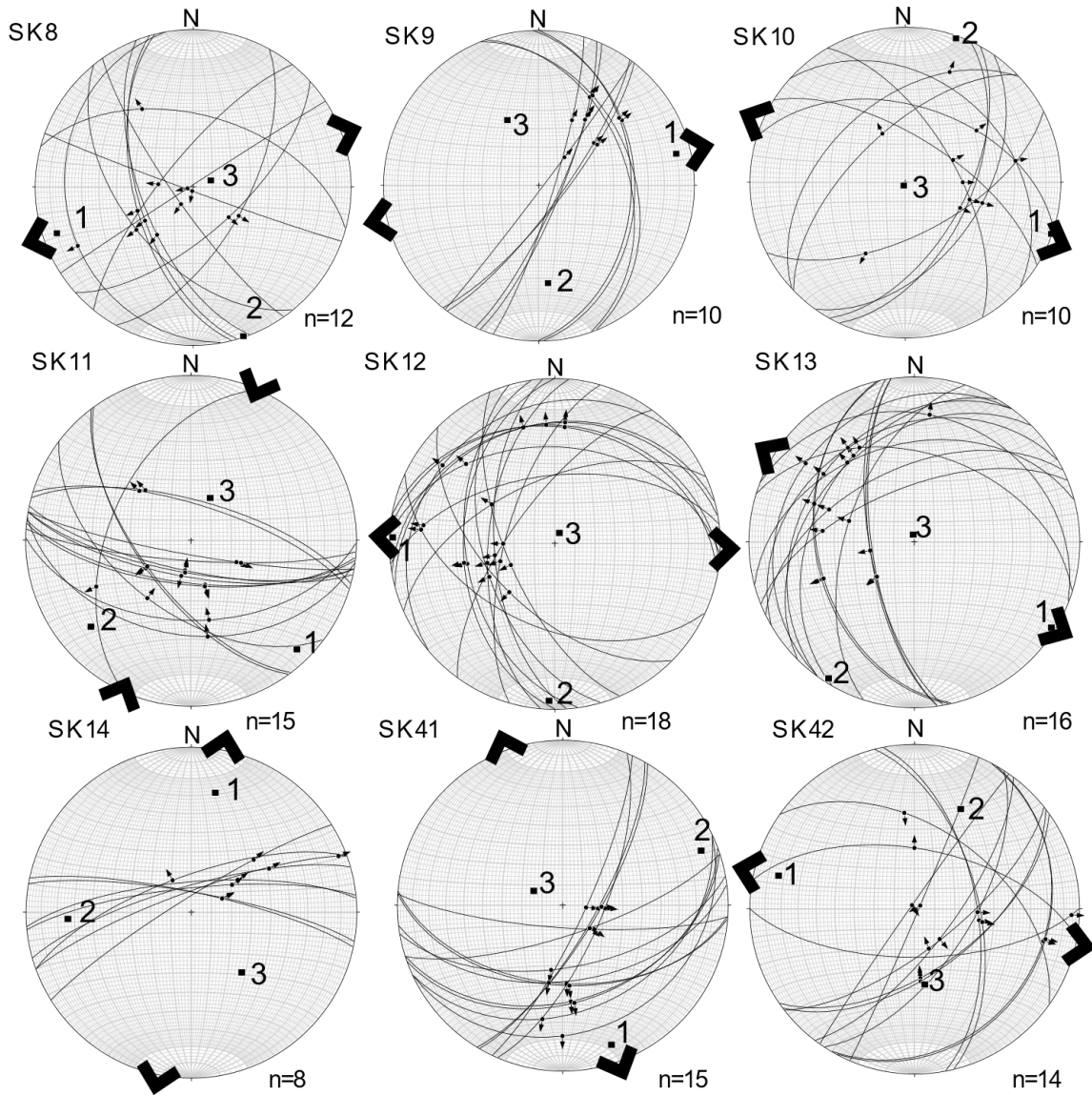


Figure 11: Fault slip data for Tochni fault zone. **SK8:** Seven normal faults dipping to the west. Two normal faults dipping to the north-west. One normal fault dipping to the north-east. Two normal faults dipping to the south-east. Overall extension west to east. **SK9:** Four normal faults dipping to the north-east. Six normal faults dipping to the south-east. Overall north-east to south-west extension. **SK10:** Two normal faults dipping to the north-west. One normal fault dipping to the south-east. Four normal faults dipping to the south-east. Three normal faults dipping to the north-east. Overall north-west to south-east extension. **SK11:** Two normal faults dipping to the north. Two normal faults dipping to the south-west. One normal fault dipping to the north-west. Seven normal faults dipping to the south. Four thrusts dipping to the south. Overall north-east to south-west shortening. **SK12:** Nine normal faults dipping to the north-west. Six normal faults dipping to the west. Three normal faults dipping to the south-west. Overall west-east extension. **SK13:** Eight normal faults dipping to the north-west. Six normal faults dipping to the west. Two normal faults dipping to the north-east. Overall north-west to south-east extension. **SK14:** Two normal faults dipping to the north-east. Six normal faults dipping to the north-west. Overall north-east to south-west extension. **SK41:** Six normal faults dipping to the south-west. Nine normal faults dipping to the south. Overall south-east to north-west extension. **SK42:** Five normal faults dipping to the west. One normal fault dipping to the north. One normal fault dipping to the south-east. Four thrusts dipping to the south-east. One thrust dipping to the north-east. One thrust dipping to the north-west. Overall south-east to north-west extension.

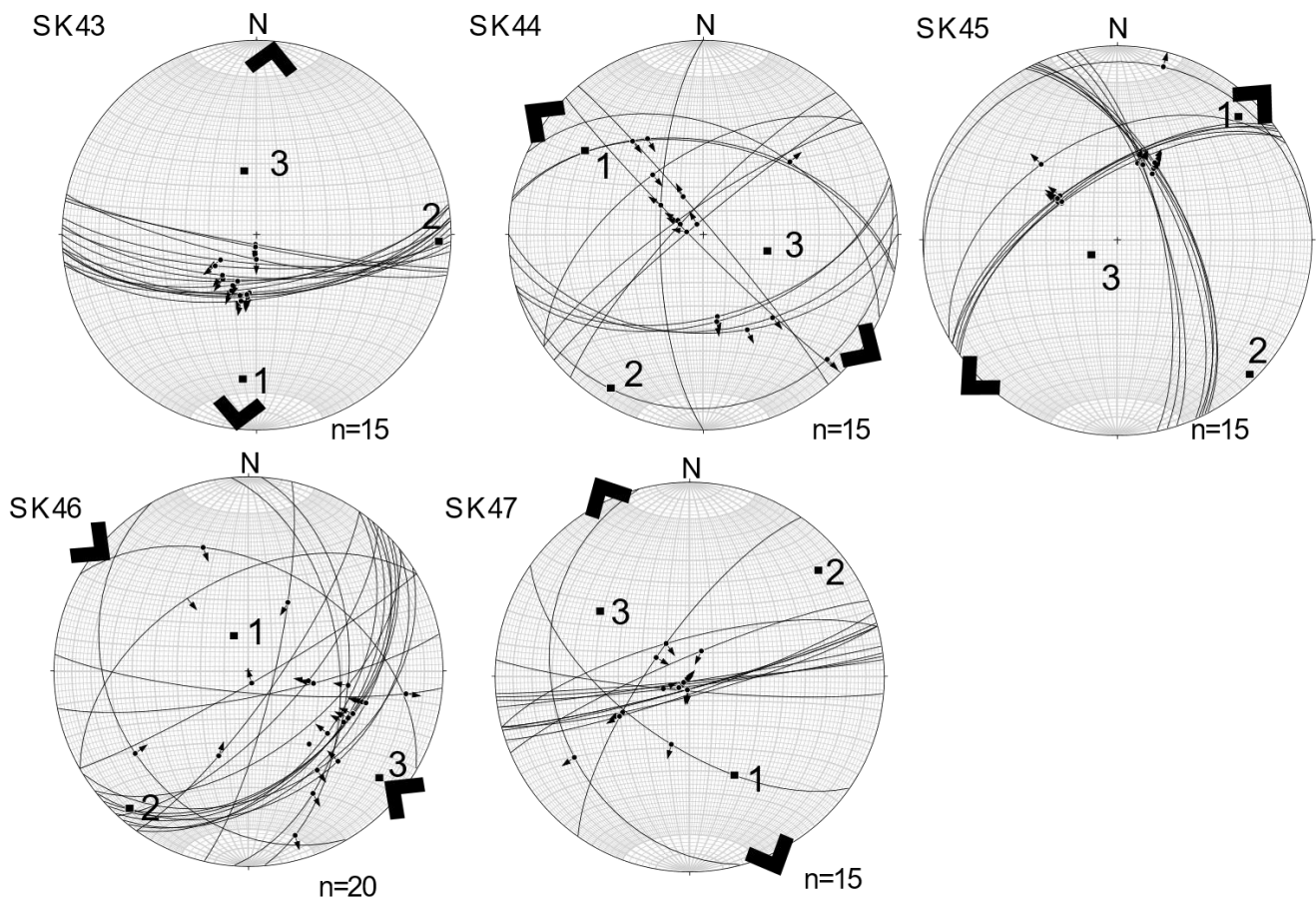


Figure 11 (continued): **SK43:** Fifteen normal faults dipping to the south. Overall north-south extension. **SK44:** Five normal faults dipping to the south. Four normal faults dipping to the north-west. One normal fault dipping to the north-east. Overall north-west to south-east extension. One thrust dipping to the north-west. Two thrusts dipping to the north-east. One sinistral strike slip fault dipping to the north-east. One dextral strike slip fault dipping to the south-west. **SK45:** Seven normal faults dipping to the north-west. Eight normal faults dipping to the north-east. Overall north-east to south-west extension. **SK46:** One thrust dipping to the north-west. One thrust dipping to the north-east. One thrust dipping to the south-west. Three thrusts dipping to the south-west. Three thrusts dipping to the west. Seven thrusts dipping to the south-east. Three normal faults dipping to the east. One dextral strike slip fault dipping to the south. Overall north-west to south-east shortening. **SK47:** Two normal faults dipping to the south-west. Two normal faults dipping to the south-east. Overall north-south to south-east extension. Three thrusts dipping to the north-west. Five thrusts dipping to the south. Two sinistral strike slip faults dipping to the south-east.

4.1 Summary and interpretation of fault-slip data

The results of the fault-slip data from the six studied fault zones suggest coeval N-S shortening and E-W extension. The data from the E-W striking Arakapas fault zone mainly show north-south shortening with simultaneous, west-east extension. Therefore, the Arakapas fault zone is interpreted as a reverse fault. However, some data indicate north-south extension which is not fully understood. Since the Arakapas fault zone has a long history dating back to deformation during seafloor spreading (Robert J varga et al 1990), it is possible that the conflicting data relate to earlier deformation events. Data from the E-W striking Wenogeia fault zone shows north-south shortening. The Wenogeia fault zone appears to be a reverse fault. The fault-slip data from the NW striking Yerasa fault zone also revealed north-south shortening and west-east extension. These kinematics suggest dextral strike-slip faulting along the NW-striking Yerasa fault zone. A fraction of fault slip data show north-south extension, which again is not fully understood but probably best constrained when viewed as an earlier deformation event. Most of the fault-slip data from the N-S striking Kalavastos, Skarinou and Tochni fault zones support west-east extension. Some data sets from the Tochni and Skarinou fault zones also show north-south extension. As a result those fault zones appear to be normal faults, and the N-S extension component may suggest a slight flattening component resulting in extension in two directions.

5. Discussion

What can the constrain of the kinematics in variably oriented fault zones, and timing of these fault zones after the investigation of the stratigraphic ages of bedrock that have been faulted in the southeast corner of the Troodos uplift, reveal? Can they shed light on possible correlation between the N-S compression and the Eratosthenes seamount collision with the uplift of Troodos mountains?

Most of the data sets show N-S shortening or E-W extension simultaneously. The E-W striking Arakapas and Wenogeia faults appear to be reverse faults, while the N-S striking Kalavassos, Tochni, Skarinou faults are normal faults. Finally, the Yerasa fault zone is interpreted to be a dextral strike-slip fault. The stratigraphic ages of the rock hosting 5 of the 6 fault zones are as young as Messinian (about 5-6 Ma) (Kinnaird, Robertson and Morris, 2011). Because most fault-slip data sets are interpreted to result from a single deformation event, this event must be younger than 5-6 Ma. This timing would allow to link that the fault-slip data with the collision of the Eratosthenes seamount with Cyprus at 1.5-2 Ma (Kempler, 1998). Consequently, the N-S shortening exerted by the collision between the Eratosthenes seamount and Cyprus causing spatially restricted shortening and increased uplift of the Troodos mountains is interpreted. The uplifting of the mountains caused differential movement and this differential motion was in part accommodated by E-W extension.

5.1 Comparison with the Ovgos fault zone

The Ovgos fault zone is a W-E striking fault zone, which formed due to north-south compression (figure 2)(Harrison *et al.*, 2004). Much like the two W-E striking fault zones this study investigated (Arakapas, Wenogeia), the Ovgos fault zone appears also to be a reverse fault. Fault-slip data in all three fault zones showcase similar results, and that would help constrain the uplift of Troodos mountains. Even though the Ovgos fault zone has not played any role in the uplift of the Troodos mountains, the origin of both fault zones is the same. Both fault zones are caused by N-S compression, and by observing similar patterns in both fault zones, a correlation can be formed. By looking at Figure 1 one can see that the uplifted volume of the Troodos mountains is much larger than of the Kyrenia range. Troodos mountains seem to have been uplifted in a greater scale. A possible interpretation to this would be that the Eratosthenes collision with Cyprus would cause this increased uplift, in contrary to the north part of Cyprus, where the N-S compression has a lesser effect in the absence of a forefront like the Eratosthenes seamount. Fault-slip data from the Arakapas and Wenogeia fault zone showed north-south shortening (figure 12). The Ovgos fault-slip data showed also N-S shortening (R.W Harrison et al 2002) (figure

13). Fault-slip from Arakapas show shallow to steep north and south dipping reverse faults, while Wenogeia shows steep north dipping reverse faults. Ovgoods fault zone data show steep north dipping reverse faults.

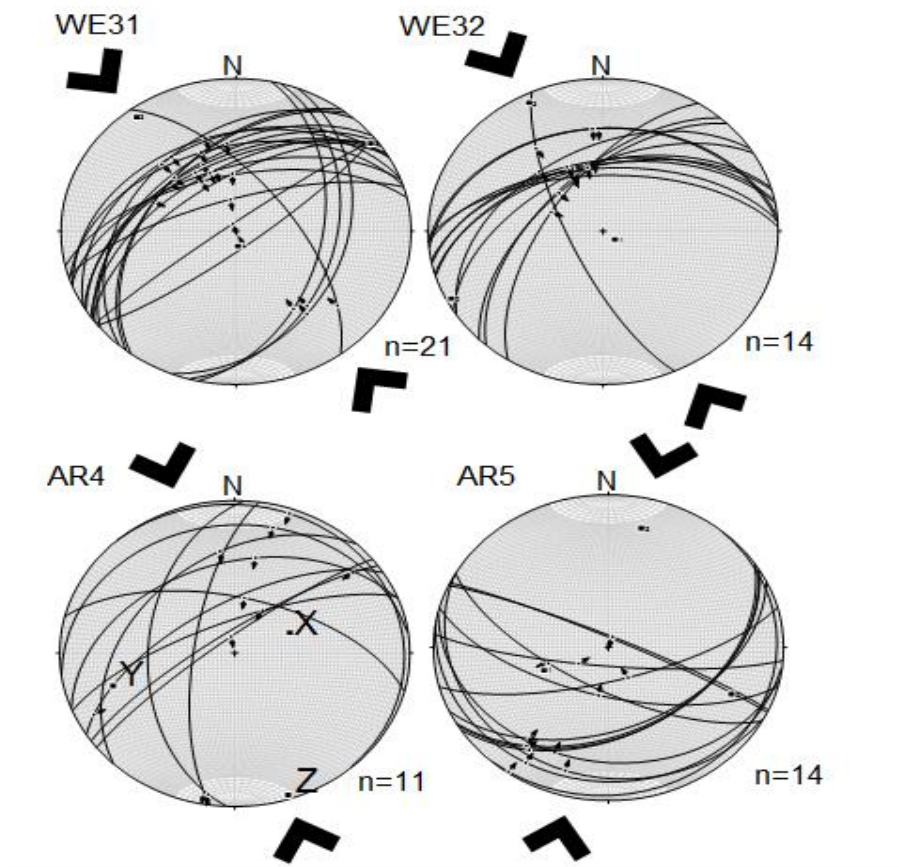


Figure 12: WE31, WE32: Fault slip data from Wenogeia fault. Both outcrops showcase mainly thrusts dipping to the northwest. AR4, AR5: fault slip data from Arakapas fault. Thrusts dipping to the northwest show a N-S shortening. AR4: Fault-slip data from Arakapas zone with thrusts dipping to the north and northwest. N-S shortening overall. AR5: Fault slip data from Arakapas fault zone showing southwest dipping thrusts showcasing N-S shortening.

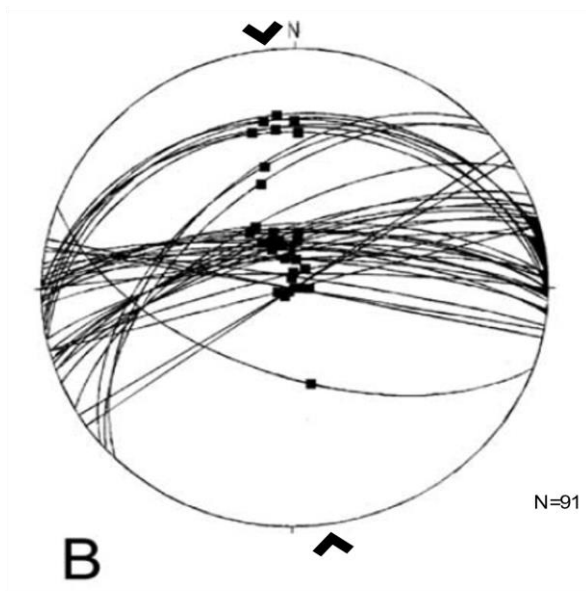


Figure 13: *B: Fault slip data from Ovgos fault zone, Thrust and high angle Thrusts dipping to the North/Northwest. (R.W. Harrison et al 2003) Overall N-S shortening (stereonet modified from R.W.Harrison et al 2003).*

5.2 Conflicting data

In the investigation certain fault-slip data was unexpected as it was contradictory to the aims of this study. These unexpected results were the following: Kalavassos outcrops with numbers 51 and 28, Arakapas outcrop with number 39 and Skarinou outcrops with numbers 14, 41, 47, 43. The fault-slip analysis focus was to link the results of the data to N-S compression. North-south compression would cause thrust faults in the E-W striking fault zones and normal fault extension on the N-S striking zones. In the results it appears that the KA51 and KA28 outcrops indicate a W-E shortening, contrary to an expected W-E extension. In the Arakapas fault-slip data AR39 appears to showcase normal fault extension to the N-S, while thrust faults that showcase N-S shortening, dictate the main pattern. Lastly

the skarinou fault-slip data revealed N-S extension instead of N-S shortening. These results can be interpreted in different ways. For the Arakapas fault zone that dates to Cretaceous those results can be indicators of older events that are not fully understood. For the contradicting results in Kalavassos and Skarinou fault, the cause could be that rock under compression can fracture in many directions (Hoek & Bieniawski, 1984) a process that could possibly cause some contradicting results throughout the fault zones.

5.3 Implications for future studies

The fault-slip data results correlated well with the Eratosthenes-Cyprus collision but there are research aspects that can be studied further. For the specific event of Eratosthenes-Cyprus collision areas east and north-east of Troodos mountains should be studied. Since the bedrock there should host fault zones caused by the uplift of the mountains, fault-slip data there could reveal more information in the event of the Eratosthenes collision with Cyprus. In practical terms, better and more concrete measurements can be taken if outcrops that are positioned off road are visited and studied. This study was limited to outcrops close, and/or by, the road. Outcrops closer to the fault zones, could reveal more information on the events that took place and show less unexpected results, producing a better data set. Another aspect that could be studied is earthquake data in the region, and how regional earthquakes can affect the fault zones (Harrison *et al.*, 2004). That could shed light in possible difficulties linking the fault-slip data to the Eratosthenes collision with Cyprus.

6. Conclusion

The study provided evidence for N-S shortening and E-W extension along variably oriented fault zones south-east of Troodos mountains, caused by N-S compression. The analysis further discussed that the ages of the bedrock hosting the fault zones are as young as upper Miocene. The outcrops showed no more than just one movement events. It is then concluded that the fault-slip data can broadly be linked with the collision between the Eratosthenes seamount and Cyprus (1.5-2 Ma). On further discussion the study compared fault-slip data from south-east of Troodos and from the Ovgos fault zone in Kyrenia range and concluded that the Troodos mountains have been uplifted higher than the Kyrenia mountains.

Acknowledgements

This project would not be possible without the guidance and extreme patience of my supervisor Uwe Ring, whom his teachings transcended geology. The support and help I received from Reuben Hansman was precious and critical to the completion of my bachelor thesis. To my family: My parents, sister and cousin. To the people who supported me throughout this project: Stylianos Iliadis, Nathalia Joukova, Nikolas Leventis, Alexandre Peillod and Eirini Makopoulou.

References

- Harrison, R. W. *et al.* (2004) 'Tectonic framework and Late Cenozoic tectonic history of the northern part of Cyprus: Implications for earthquake hazards and regional tectonics', *Journal of Asian Earth Sciences*, 23(2), pp. 191–210. doi: 10.1016/S1367-9120(03)00095-6.
- Kempler, D. (1998) '53 . ERATOSTHENES SEAMOUNT : THE POSSIBLE SPEARHEAD OF INCIPIENT CONTINENTAL', *Proceedings of the Ocean Drilling Program, Scientific Results*, 160.
- Kinnaird, T. C., Robertson, a. H. F. and Morris, a. (2011) 'Timing of uplift of the Troodos Massif (Cyprus) constrained by sedimentary and magnetic polarity evidence', *Journal of the Geological Society*, 168(2), pp. 457–470. doi: 10.1144/0016-76492009-150.
- Mart, Y. and Ryan, W. B. F. (2002) 'The complex tectonic regime of the Cyprus Arc: A short review', *Israel Journal of Earth Sciences*, 51(January), pp. 117–134. doi: 10.1560/DCF4-08Q2-UF1U-6QK5.
- Petit, J. P. (1987) 'Criteria for the sense of movement on fault surfaces in brittle rocks', *Journal of Structural Geology*, 9(5–6), pp. 597–608. doi: 10.1016/0191-8141(87)90145-3.
- Robertson, A. H. F. (1998) '51. Formation and Destruction of the Eratosthenes Seamount, Eastern Mediterranean Sea, and Implications for Collisional Processes', *Proceedings of the Ocean Drilling Program, Scientific Results*, 160, pp. 681–699.
- Varga, R. J. (1991) 'Modes of extension at oceanic spreading centers: evidence from the Solea graben, Troodos ophiolite, Cyprus', *Journal of Structural Geology*, 13(5), pp. 517–537. doi: 10.1016/0191-8141(91)90041-G.
- 'Brittle fracture propagation in rock under compression'
- Hoek, E. & Bieniawski, Z.T. *Int J Fract* (1984) 26: 276. doi:10.1007/BF00962960
- NASA JPL. (2013). NASA Shuttle Radar Topography Mission Global 1 arc second [Data set]. NASA LP DAAC. <https://doi.org/10.5067/MEaSURES/SRTM/SRTMGL1.003>

Appendix

Coordinates, outcrop numbers along with number of measurements can be seen in this section.

Eigenvalues, Trend and plunge calculations from the Faultkin program are presented in this section.

1. Arakapas fault zone

Coordinates N345132 E0325448.5

Outcrop number 40

Number of measurements 15

Axis	Eigenvalue	Trend	Plunge
1.	0.1529	259.0,	16.9
2.	0.0859	350.5,	04.7
3.	0.2388	095.5,	72.4

Coordinates N345227 E0325505.5

Outcrop number 39

Number of measurements 20

Axis	Eigenvalue	Trend	Plunge
1.	0.1101	190.4,	17.1
2.	0.0927	282.0,	04.9
3.	0.2028	027.2,	72.1

Coordinates N345032 N0331536

Outcrop number 30

Number of measurements 14

Axis	Eigenvalue	Trend	Plunge
1.	0.3660	230.5,	02.2
2.	0.0444	320.5,	00.3
3.	0.3216	058.8,	87.8

Coordinates N345022 N0331110

Outcrop number 27

Number of measurements 11

Axis	Eigenvalue	Trend	Plunge
1.	0.2387	052.0,	09.8
2.	0.0587	155.3,	53.3
3.	0.1800	315.1,	34.9

Coordinates N345036 E0330819

Outcrop number 26

Number of measurements 15

Axis	Eigenvalue	Trend	Plunge
1.	0.1856	204.2,	70.9
2.	0.0311	104.8,	03.2
3.	0.2167	013.7,	18.8

Coordinates N345105 E0330315.5

Outcrop number 25
Number of measurements 14

Axis	Eigenvalue	Trend	Plunge
1.	0.2939	194.4,	07.1
2.	0.0072	285.8,	10.6
3.	0.3011	071.4,	77.2

Coordinates N345116.5 E0330245
Outcrop number 24
Number of measurements 10

Axis	Eigenvalue	Trend	Plunge
1.	0.2587	113.3,	08.1
2.	0.0287	209.1,	35.4
3.	0.2874	012.2,	53.4

Coordinates N345101 E0330206
Outcrop number 23
Number of measurements 10

Axis	Eigenvalue	Trend	Plunge
1.	0.2711	188.4,	16.5
2.	0.0492	086.3,	35.3
3.	0.3203	299.0,	49.9

Coordinates N344806 E0330906
Outcrop number 6
Number of measurements 15

Axis	Eigenvalue	Trend	Plunge
1.	0.2843	258.5,	04.1
2.	0.0643	166.8,	22.8
3.	0.3487	358.0,	66.8

Coordinates N345044 E0330904
Outcrop number 5
Number of measurements 14

Axis	Eigenvalue	Trend	Plunge
1.	0.3264	247.6,	57.3
2.	0.0130	113.4,	24.1

3. 0.3134 013.7, 20.7

Coordinates N395034.5 E0330656

Outcrop number 4

Number of measurements 11

Axis	Eigenvalue	Trend	Plunge
1.	0.2339	067.1,	61.7
2.	0.0143	252.9,	28.2
3.	0.2482	161.6,	02.4

2.Yerasa fault zone

Coordinates N344528 E0330506

Outcrop number 1

Number of measurements 15

Axis	Eigenvalue	Trend	Plunge
1.	0.3962	025.0,	76.5
2.	0.0022	279.9,	03.6
3.	0.3940	189.1,	13.0

Coordinates N344603 E0330447

Outcrop number 2

Number of measurements 14

Axis	Eigenvalue	Trend	Plunge
1.	0.3585	290.9,	79.9
2.	0.0524	098.1,	09.9
3.	0.3061	188.5,	02.2

Coordinates N344629 E0330445

Outcrop number 3

Number of measurements 14

Axis	Eigenvalue	Trend	Plunge
1.	0.3623	264.9,	00.6
2.	0.0514	355.0,	06.9
3.	0.4137	169.7,	83.1

Coordinates N344320.5 E0330807.2

Outcrop number 54

Number of measurements 18

Axis	Eigenvalue	Trend	Plunge
1.	0.4707	087.7,	38.2
2.	0.0147	187.6,	12.4
3.	0.4854	292.4,	49.1

Coordinates N344327.9 E0330821.2

Outcrop number 53

Number of measurements 16

Axis	Eigenvalue	Trend	Plunge
1.	0.3692	162.7,	03.9
2.	0.1179	253.3,	09.0
3.	0.4871	049.7,	80.2

Coordinates N344347 E0330843.1
 Outcrop number 52
 Number of measurements 21

Axis	Eigenvalue	Trend	Plunge
1.	0.3615	068.0,	02.7
2.	0.0239	337.3,	13.9
3.	0.3854	168.9,	75.8

Coordinates N344740.6 E0330457.1
 Outcrop number 38
 Number of measurements 12

Axis	Eigenvalue	Trend	Plunge
1.	0.3820	208.5,	05.4
2.	0.0114	118.3,	01.6
3.	0.3934	012.0,	84.4

Coordinates N344442 E0330451
 Outcrop number 37
 Number of measurements 15

Axis	Eigenvalue	Trend	Plunge
1.	0.2984	138.1,	10.8
2.	0.0262	046.7,	07.5
3.	0.3245	282.6,	76.8

Coordinates N344351 E0330022.5
 Outcrop number 22
 Number of measurements 15

Axis	Eigenvalue	Trend	Plunge
1.	0.3427	269.6,	11.1
2.	0.0216	179.4,	01.0
3.	0.3643	084.1,	78.9

Coordinates N344351 E0330022.5
 Outcrop number 21
 Number of measurements 15

Axis	Eigenvalue	Trend	Plunge
1.	0.1660	287.8,	75.7
2.	0.0172	088.2,	13.5
3.	0.1833	179.3,	04.6

Coordinates N344752 E0325958
 Outcrop number 20
 Number of measurements 13

Axis	Eigenvalue	Trend	Plunge
1.	0.2005	268.8,	19.9
2.	0.0309	125.6,	65.6
3.	0.1696	003.8,	13.4

Coordinates N344810 E0330037
 Outcrop number 19
 Number of measurements 19

Axis	Eigenvalue	Trend	Plunge
1.	0.2207	132.1,	42.6
2.	0.0180	226.7,	05.0
3.	0.2386	322.1,	47.0

Coordinates N344745 E0330139
 Outcrop number 18
 Number of measurements 12

Axis	Eigenvalue	Trend	Plunge
1.	0.1769	235.1,	18.2
2.	0.0405	325.1,	00.0
3.	0.2174	055.3,	71.8

Coordinates N344649 E0330240.5
 Outcrop number 17
 Number of measurements 14

Axis	Eigenvalue	Trend	Plunge
1.	0.2388	048.9,	19.5
2.	0.0832	141.0,	05.8
3.	0.1556	246.8,	69.6

3.Kalavastos fault zone

Coordinates N344610.6 E0331756.9

Outcrop number 51

Number of measurements 16

Axis	Eigenvalue	Trend	Plunge
1.	0.2400	332.5,	54.2
2.	0.0755	207.6,	22.5
3.	0.1645	105.8,	26.3

Coordinates N344748.5 E0331652

Outcrop number 29

Number of measurements 15

Axis	Eigenvalue	Trend	Plunge
1.	0.1705	076.1,	04.5
2.	0.0001	345.8,	03.9
3.	0.1706	215.0,	84.0

Coordinates N344627 E03318052

Outcrop number 28

Number of measurements 13

Axis	Eigenvalue	Trend	Plunge
1.	0.1779	059.8,	47.7
2.	0.0107	184.9,	27.6
3.	0.1672	291.9,	29.2

4.Tochni fault zone

Coordinates N344659.1 E0331920.5

Outcrop number 50

Number of measurements 21

Axis	Eigenvalue	Trend	Plunge
1.	0.2838	253.2,	33.1
2.	0.0761	162.9,	00.4
3.	0.3599	072.2,	56.9

Coordinates N344533.9 E0332023.8

Outcrop number 49

Number of measurements 21

Axis	Eigenvalue	Trend	Plunge
1.	0.4043	341.2,	21.4
2.	0.0614	071.8,	01.7
3.	0.4657	166.1,	68.5

Coordinates N344533.9 E0332023.8
Outcrop number 48
Number of measurements 15

Axis	Eigenvalue	Trend	Plunge
1.	0.3777	021.1,	18.4
2.	0.0166	290.9,	00.6
3.	0.3943	199.0,	71.6

Coordinates N344532 E0332049
Outcrop number 16
Number of measurements 22

Axis	Eigenvalue	Trend	Plunge
1.	0.1579	265.3,	11.0
2.	0.1160	174.7,	03.2
3.	0.2739	068.8,	78.5

Coordinates N344532 E0332049
Outcrop number 15
Number of measurements 10

Axis	Eigenvalue	Trend	Plunge
1.	0.4032	062.6,	27.3
2.	0.0775	331.3,	02.6
3.	0.3258	236.2,	62.5

Coordinates N344657 E0332049
Outcrop number 7
Number of measurements 5

Axis	Eigenvalue	Trend	Plunge
1.	0.4562	279.2,	17.6
2.	0.0019	010.2,	03.3
3.	0.4582	110.4,	72.1

6.Skarinou fault zone

Coordinates N344928.7 E0332127.4
Outcrop number 47
Number of measurements 15

Axis	Eigenvalue	Trend	Plunge
1.	0.0634	155.4,	43.7
2.	0.0623	050.5,	15.1
3.	0.1256	306.2,	42.5

Coordinates N344923.6 E0332132.4
Outcrop number 46
Number of measurements 20

Axis	Eigenvalue	Trend	Plunge
1.	0.2819	338.1,	74.0
2.	0.0795	220.9,	07.5
3.	0.2024	129.0,	14.1

Coordinates N344921.2 E0332137.2
Outcrop number 45
Number of measurements 15

Axis	Eigenvalue	Trend	Plunge
1.	0.2566	044.5,	11.8
2.	0.1379	135.2,	03.3
3.	0.3945	240.6,	77.7

Coordinates N344827.9 E0332300.2
Outcrop number 44
Number of measurements 15

Axis	Eigenvalue	Trend	Plunge
1.	0.1408	305.5,	26.3
2.	0.0769	211.1,	08.8
3.	0.2177	104.1,	62.0

Coordinates N344802 E0332357
Outcrop number 43
Number of measurements 15

Axis	Eigenvalue	Trend	Plunge
1.	0.4788	185.3,	26.4
2.	0.0027	092.1,	06.5
3.	0.4761	349.3,	62.6

Coordinates N344830.7 E0332325
Outcrop number 42
Number of measurements 14

Axis	Eigenvalue	Trend	Plunge
1.	0.1607	283.8,	16.2
2.	0.0467	024.9,	33.6
3.	0.1139	172.2,	51.7

Coordinates N345132 E0325443
Outcrop number 41
Number of measurements 15

Axis	Eigenvalue	Trend	Plunge
1.	0.3356	160.6,	11.5
2.	0.0746	068.4,	10.7
3.	0.4103	296.8,	74.2

Coordinates N344807 E0332309
Outcrop number 14
Number of measurements 8

Axis	Eigenvalue	Trend	Plunge
1.	0.4513	011.5,	27.0
2.	0.0341	266.9,	26.2
3.	0.4172	139.9,	50.7

Coordinates N344807 E0332309
Outcrop number 13
Number of measurements 16

Axis	Eigenvalue	Trend	Plunge
1.	0.2979	121.9,	02.3
2.	0.1131	212.1,	02.9
3.	0.4111	353.9,	86.3

Coordinates N344827 E0332260
Outcrop number 12
Number of measurements 18

Axis	Eigenvalue	Trend	Plunge
1.	0.2373	272.2,	02.2
2.	0.1593	182.0,	05.3
3.	0.3967	024.6,	84.2

Coordinates N344956.5 E0332059
Outcrop number 11
Number of measurements 15

Axis	Eigenvalue	Trend	Plunge
1.	0.0703	135.7,	08.8
2.	0.0099	229.2,	21.2
3.	0.0802	024.5,	66.9

Coordinates N344928 E0332143
Outcrop number 10

Number of measurements 10

Axis	Eigenvalue	Trend	Plunge
1.	0.2063	109.5,	00.1
2.	0.1950	019.5,	01.8
3.	0.4013	202.5,	88.2

Coordinates N344928 E0332143

Outcrop number 9

Number of measurements 10

Axis	Eigenvalue	Trend	Plunge
1.	0.3914	077.0,	09.9
2.	0.0674	174.5,	36.8
3.	0.4588	334.4,	51.4

Coordinates N344928 E0332143

Outcrop number 8

Number of measurements 12

Axis	Eigenvalue	Trend	Plunge
1.	0.2217	251.3,	09.8
2.	0.1018	161.3,	00.3
3.	0.3236	069.6,	80.2

6. Wenogea fault zone

Coordinates N344917.2 E0331956.6

Outcrop number 36

Number of measurements 15

Axis	Eigenvalue	Trend	Plunge
1.	0.2844	112.5,	73.1
2.	0.0505	229.2,	07.8
3.	0.2339	321.3,	14.9

Coordinates N345012 E0332159

Outcrop number 35

Number of measurements 14

Axis	Eigenvalue	Trend	Plunge
1.	0.4056	072.7,	78.2
2.	0.0141	220.2,	10.0
3.	0.3915	311.3,	06.2

Coordinates N345044.7 E0332156.5

Outcrop number 34
Number of measurements 15

Axis	Eigenvalue	Trend	Plunge
1.	0.3904	265.3,	11.0
2.	0.0336	356.0,	03.4
3.	0.4240	102.9,	78.5

Coordinates N345050 E0332237.7
Outcrop number 33
Number of measurements 15

Axis	Eigenvalue	Trend	Plunge
1.	0.3625	271.4,	03.4
2.	0.0353	001.4,	01.2
3.	0.3271	111.3,	86.4

Coordinates N345100 E0332239
Outcrop number 32
Number of measurements 14

Axis	Eigenvalue	Trend	Plunge
1.	0.4416	127.5,	82.8
2.	0.0317	243.0,	03.1
3.	0.4099	333.4,	06.5

Coordinates N345001 E0332050.5
Outcrop number 31
Number of measurements 21

Axis	Eigenvalue	Trend	Plunge
1.	0.4208	173.1,	82.1
2.	0.0259	053.3,	04.0
3.	0.3949	322.8,	06.9